Treatment of human pancreatic cancer using combined ultrasound, microbubbles and gemcitabine: a clinical case study.

Spiros Kotopoulis[1,2 *], Georg Dimcevski[1,3], Odd Helge Gilja[1,3], Dag Hoem[4], Michiel Postema[2,5]

[1] National Centre for Ultrasound in Gastroenterology, Haukeland University Hospital, Bergen, Norway

[2] Department of Physics and Technology, University of Bergen, Bergen, Norway

[3] Department of Clinical Medicine, University of Bergen, Bergen, Norway

[4] Department of Surgery, Haukeland University Hospital, Bergen, Norway

[5] The Michelsen Centre for Industrial Measurement Science and Technology, Bergen, Norway

Abstract

Purpose: The purpose of this study was to investigate the ability and efficacy of inducing sonoporation in a clinical setting, using commercially available technology, to increase the patients' quality of life and extend the low ECOG performance grade; as a result increasing the overall survival in patients with pancreatic adenocarcinoma.

Methods: Patients were treated using a customised configuration of a commercial clinical ultrasound scanner over a time period of 31.5 min following standard chemotherapy treatment with gemcitabine. SonoVue® ultrasound contrast agent was injected intravascularly during the treatment with the aim to induce sonoporation.

Results: Using our custom acoustic settings, our patients were able to undergo an increased number of treatment cycles; from an average of 9 to 16 cycles when

* **Corresponding author email: Spiros.Kotopoulis@uib.no**

comparing to a historical control group of 80 patients. In two out of five patients treated, the maximum tumour diameter was temporally decreased to 80±5% and permanently to 70±5% of their original size, whilst the other patients showed reduced growth.

We also explain and characterise the settings and acoustic output obtained from a commercial clinical scanner used for combined ultrasound microbubble and chemotherapy treatment.

Conclusion: It is possible to combine ultrasound, microbubbles, and chemotherapy in a clinical setting using commercially available clinical ultrasound scanners to increase the number of treatment cycles, prolonging the quality of life in patients with pancreatic adenocarcinoma compared to chemotherapy alone.

Purpose

Cancer is the world's second largest cause of death with over 7.6 million deaths a year (21% of NCD deaths) [1]. There are over 217 000 new cases of pancreatic cancer worldwide every year [2]. Pancreatic cancer is very difficult to treat due to its aggressive biology, late diagnosis, the encasement of large blood vessels, and the presence of metastasis. Hence, surgery is rarely an option. Chemotherapy produces modest responses but is not curative in this setting, mainly because its use is severely hampered by toxic effects to vital organs. As a result, the survival is very low. The mortality of the inoperable patients is 50% within 3 months and 90% within 12 months [3, 4].

Sonoporation is a novel method for non-invasive targeted drug and gene delivery [5-8]. Sonoporation is defined as the transient formation of pores in cell membranes owing to ultrasound or a combination of ultrasound and microbubbles. These pores range in size from several nanometres to several micrometres [9-12], allowing for increased drug uptake in highly targeted regions [13-15].

The acoustic parameters used for sonoporation showing increased cellular uptake of chemotherapeutics and genes vary from low-intensity diagnostic ultrasound (Mechanical Index (MI) < 0.3) [16-29] to high-intensity diagnostic ultrasound (MI > 1.0) [9, 30-34]. Throughout literature, the acoustic settings used to induce sonoporation vary drastically, with a broad range of these settings showing improved drug and gene delivery. Several studies also show the effect of clinical diagnostic ultrasound in standard colour-Doppler and B-mode imaging on cellular uptake [19, 20]. These studies, which made use of clinical diagnostic scanners, concluded that a larger duty cycle was necessary to increase the effect of sonoporation. It has been

shown that the ideal settings to induce sonoporation are when shock-waves were not present, in order to sustain the microbubbles, and when the duty cycle is long enough, to excite the microbubbles in the targeted area without heating the surrounding tissue [16]. Furthermore, higher intensities correlating to cavitation and jetting result in increased cell death due to mechanical damage instead of (transient) sonoporation [33, 35-37]. As a result, there is no consensus on the exact ultrasound settings to be used for sonoporation [38]. For this reason we aimed to use settings that matched our previous *in-vitro* and *in-vivo* work as much as possible, *i.e.,* an *in-situ* MI=0.2, maximum duty cycle, and minimum shockwave generation in order to preserve the microbubbles [7, 8, 23].

To date, all sonoporation experiments have been done either *in vitro* or in animal models, hence the effect of sonoporation in humans is not truly known yet.

Ultrasound has been used as a tool in the clinic for many years, especially in transabdominal imaging. Specifically, the pancreas can easily be imaged ultrasonically [39]. In clinical ultrasonic imaging, ultrasound is combined with so-called ultrasound contrast agents to locate tumours [40, 41]. These agents consist of gas microbubbles encapsulated by elastic shells [42]. Using a clinical diagnostic scanner for combined imaging and treatment allows for precise acoustic field alignment ensuring that the correct ultrasound intensity reaches the target area.

In this study, we worked towards optimising the ultrasonic settings for invoking sonoporation in the target region of a pancreatic tumour using a common commercial clinical ultrasound scanner without physical modifications.

Methods

A clinical scanner was calibrated in a degassed water bath in order to map the beam profile and optimise the acoustic settings. After the chemotherapeutic dose was delivered, the clinical probe was positioned aiming directly at the pancreatic tumour and locked in place for 31.5 minutes. The probe was attached to a ball joint and was positioned near the upper abdomen. Stomach and intestine were avoided in all cases to ensure propagation only through soft tissue, to ensure delivery of the aimed ultrasound intensity at the desired area. Once the tumour was located the probe orientation was fine-tuned in order to locate the largest slice of the tumour and as much vasculature as possible, *i.e.,* the feeding vessels. The probe was then locked in position until the completion of the treatment. The natural breathing motion aided the treatment as the ultrasound slice gently oscillated through the tumour. By visualising the vasculature and tumour it could be ensured that the microbubbles were being sonicated at the target. These vessels were then used as a reference point for future treatments. Nine doses of ultrasound contrast agent were intravenously injected over this time period to enhance the sonoporation effect. To evaluate the efficacy of the combined treatment we compared the amount of chemotherapy cycles the patient was able to receive. Furthermore, the tumour size was measured over the course of the treatment cycles to monitor and compare the tumour growth.

Ultrasound scanner configuration

A GE LOGIQ 9 ultrasound scanner (GE Healthcare, Waukesha, WI) combined with a 4C curvilinear probe (GE Healthcare) was used for both diagnosis and therapy.

106 To calibrate and program the diagnostic scanner for the optimised therapeutic settings
107 the probe was locked in position in a custom-made 250-L 3D scanning tank,
108 containing degassed water. A calibrated HGL-200 bullet-type hydrophone (Onda,
109 Sunnyvale, CA) connected to a WaveJet 354a oscilloscope (Teledyne LeCroy SA,
110 Geneva, Switzerland) was used to measure the acoustic signal. The scanning tank had
111 a spatial resolution of 0.4 μm. For the calibration a 200-μm resolution was used.
112 AQUASONIC® ultrasound transmission gel (Parker Laboratories, Fairfield, NJ) was
113 placed on the transducer transmission surface and the probe was subsequently covered
114 using a latex ultrasound probe cover (Sheathing Technologies, Inc., Morgan Hill, CA)
115 prior to submersion. The diagnostic scanner settings were modified in order to
116 achieve a maximum duty cycle without completely degrading the image quality, in
117 addition to having a linear acoustic signal. We aimed for minimal acoustic
118 shockwaves and harmonics minimising potential cavitation. The absence of nonlinear
119 content was verified by visualising the temporal extent of the pulses and performing a
120 Fast Fourier Transform (FFT) [43]. Multiple focal depths (from 2.8 cm to 8.4 cm) and
121 different settings (varying gain, changing window size, etc.) were evaluated to ensure
122 similar acoustic conditions in all cases. To calculate the *in-situ* acoustic pressures and
123 intensities, the *in-water* values were derated by 0.3 dB/MHz/cm, an approximation of
124 soft tissue attenuation in accordance to FDA and IEC guidelines [44, 45]. The
125 attenuation factor of 0.3 dB/MHz/cm is only valid for soft tissue. Hence, this
126 calibration was representative for our clinical positioning for targeting the pancreas.
127
128 Table 1 shows the ultrasound scanner settings used to perform the simultaneous
129 observation and treatment of the pancreatic tumours. Skilled clinical sonographers
130 were called upon to judge the image quality. As there are variations between patients,

131 such as tumour depth and tissue attenuation, certain settings had to be adjusted to
132 ensure the correct ultrasound intensity reached the required area whilst maintaining
133 the image quality. The settings that were varied are labelled as *Patient-depending*.
134 The three settings that were adjusted prior to treatment were: the focal depth, image
135 depth, and gain. The focal and image depths were adjusted in order to visualise and
136 position the acoustic focus directly in the middle of the tumour. By doing so we
137 could ensure that the acoustic conditions the tumour received was as similar as
138 possible in all patients. The gain is only applied after the received signal, hence it did
139 not affect the acoustic output. The gain simply allowed for a brighter image.
140 Once the probe was locked in position and the tumour was "targeted", no changes to
141 the ultrasonic conditions were made.
142
143

	B-mode	Contrast mode			
Parameter	**Value**		**Unit**	**Description**	**Variability**
MI	0.4	0.4		Mechanical Index	None
TIs	0.0	0.0		Thermal Index of soft tissue	None
Freq	4.0	4.0	MHz	Centre Receive frequency	None
AO	1	36	%	Normalised acoustic output	None
FR	4	4	fps	Frame rate	None
Gn	30-45	30-45	dB	Gain	Patient-depending
S/A	3/3	2/0		Synthetic Aperture	None
Map	F/0	2/0		Colour map	None
F	5.2-6.8	5.2-6.8	cm	Focal depth	Patient-depending
D	10-15	10-15	cm	Image Depth	Patient-depending
DR	66	66	dB	Dynamic Range	None
SRI HD	3	3		Image smoothing	None
Grey Map	F/0	H		Image colour maps	None

Trig	-0.25	-	s	Trigger delay	None
Tint Map	D	-		Image colour maps	None
Trig	-	0-1		Image triggering	None
TAD	-	on		True Agent Detection	None
F.Average	-	3	frames	Frame averaging	None

144 **Table 1:** Parameters as indicated on a GE LOGIQ 9 clinical ultrasound scanner.

145 The settings chosen resulted in acoustic conditions shown in Table 2 and beam
146 profiles shown in Figure 1.

147

	Centre frequency (MHz)	Duty cycle (%)	Mechanical Index	Acoustic power I_{SATA} (mW/cm^2)	Peak peak-negative acoustic pressure (MPa)
in-water values at 6.7 cm depth	1.9	1 (4 cycles every 0.21 ms)	0.49	0.59	0.41
Derated *in-situ* values at 6.7 cm depth	1.9	1 (4 cycles every 0.21 ms)	0.20	0.25	0.27

148

149 **Table 2:** Acoustic conditions generated by the 4C probe for sonoporation *in-water*
150 and derated for *in-situ* values [44, 45].

151

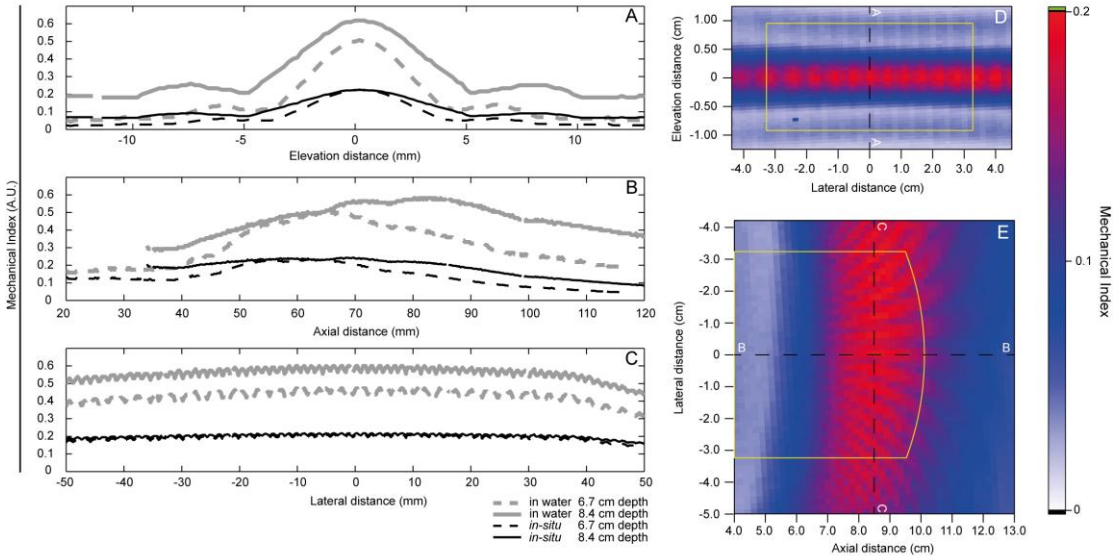

152

153 **Figure 1:** 1D and 2D beam profiles at sonoporation settings using the 4C probe at two
154 focal depths: 6.7 cm and 8.4 cm for the 1D plots and 8.4 cm for the 2D plots. The
155 beam profile was characterised in water and derated for *in-situ* values [44, 45]. Lines
156 A-A, B-B, and C-C in panels D and E represent the position of the 1D scans shown in
157 panels A, B and C respectively. The yellow bounding boxes in panels D and E
158 represent the area visible on the clinical scanner screen. In the elevation direction the
159 bounding box was defined by when a 0.5mm needle could not be distinguished on
160 screen. The tumour was positioned at the intersection of lines B-B and C-C in frame E,
161 and at an elevation distance of 0 mm in frame D.

162

163 The beam profile showed formation of multiple foci in close proximity along the
164 lateral direction merging to form a quasi-continuous focus (Figure 1E). In the
165 elevation direction side lobes can be clearly seen (Figure 1A and 1D). Using the full
166 width half maximum (FWHM) to define the beam size, the active or treatment area
167 can be defined as a volume of 69 × >100 × 1.0 $(mm)^3$ (l×w×h). It is assumed that this
168 is the region were sonoporation occurred most efficiently. Figure 2 shows the pulse

repetition pattern generated by these settings. The pulse was amplitude-modulated, consisting of 5 cycles (2.1 μs) every 210 μs corresponding to a 1% duty cycle (repetition rate optimised). The duty cycle is defined as the percentage of time that ultrasound is being generated. This was measured during the spatial calibration process, in the acoustic focus with the hydrophone, for the duration of the inverse of the frame rate. Due to synthetic aperture and contrast enhanced imaging the pulse pattern at the focus was amplitude-modulated [46] [47]. This can be seen in the upper panel of Fig. 2. The lower panel of Fig. 2 shows the time signal of a single pulse. The pulse is still relatively sine-shaped, thus the transfer function of the propagation path is linear. Minor nonlinear effects can be seen after the 4^{th} cycle. This indicates that shockwave occurrence and therefore microbubble destruction is negligible.

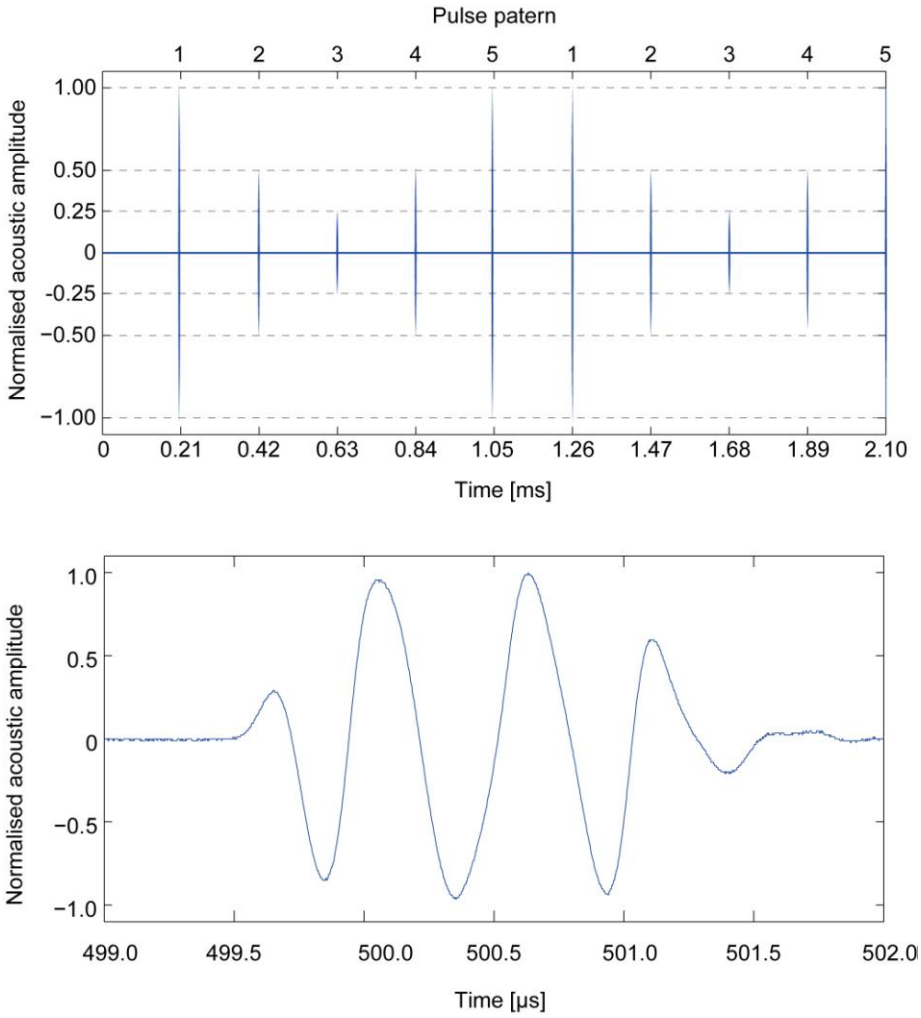

180

181 **Figure 2:** Ultrasonic pulse generated by the clinical scanner. The top panel shows the
182 pulse repetition frequency and pattern. The lower panel shows the temporal extent of
183 the pulse with the largest amplitude. The pulses were amplitude-modulated. Each
184 pulse consisted of 4 cycles (2.1 µs) every 210 µs.

185 A Fast Fourier Transform (FFT) of the acoustic signal is shown in Fig. 3. The centre
186 frequency is 1.9 MHz. Using a –3-dB or FWHM cut-off the bandwidth was measured
187 to be 1.1 MHz; from 1.3 – 2.4 MHz. A second harmonic peak can be seen at 3.6 MHz
188 due to the minor non-linear effects. This peak was 11 dB lower than the primary peak.

189

These settings complied with current safety guidelines for clinical diagnostic imaging [44, 48, 49]. Figure 4 shows two images of pancreatic cancer in two separate patients captured using the sonoporation treatment settings.

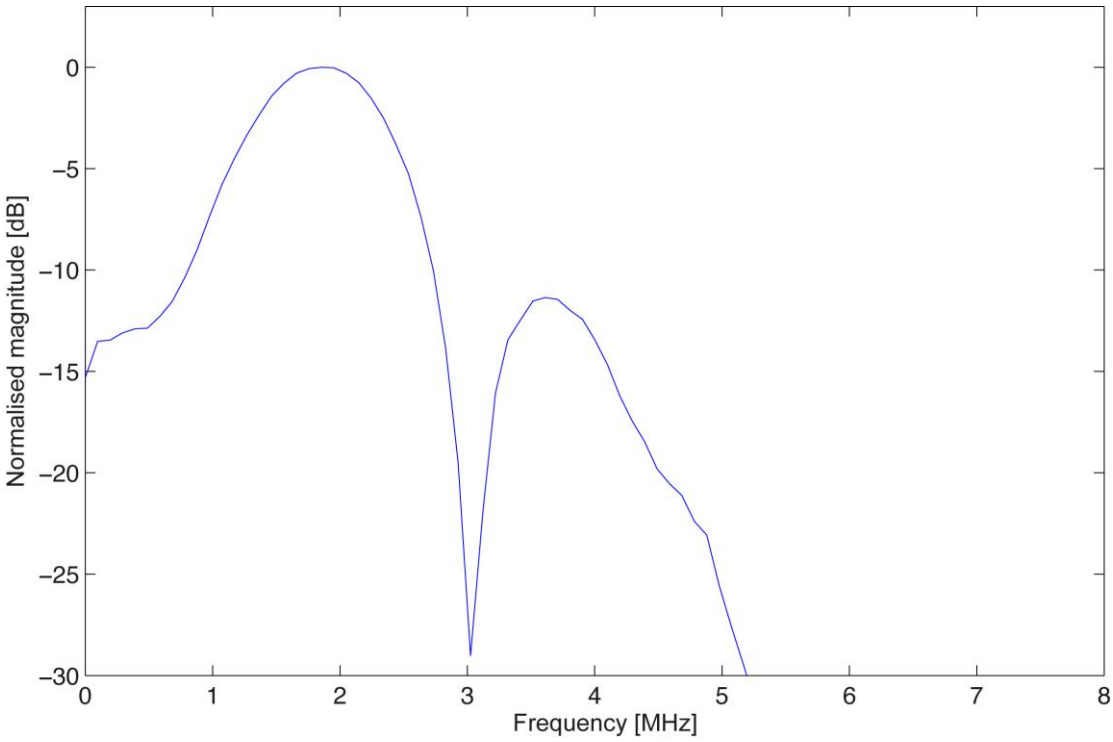

Figure 3: Fast Fourier transform of ultrasonic signal. The centre frequency of the transmitted signal is 1.9 MHz. A bandwidth of 1.1 MHz can be seen.

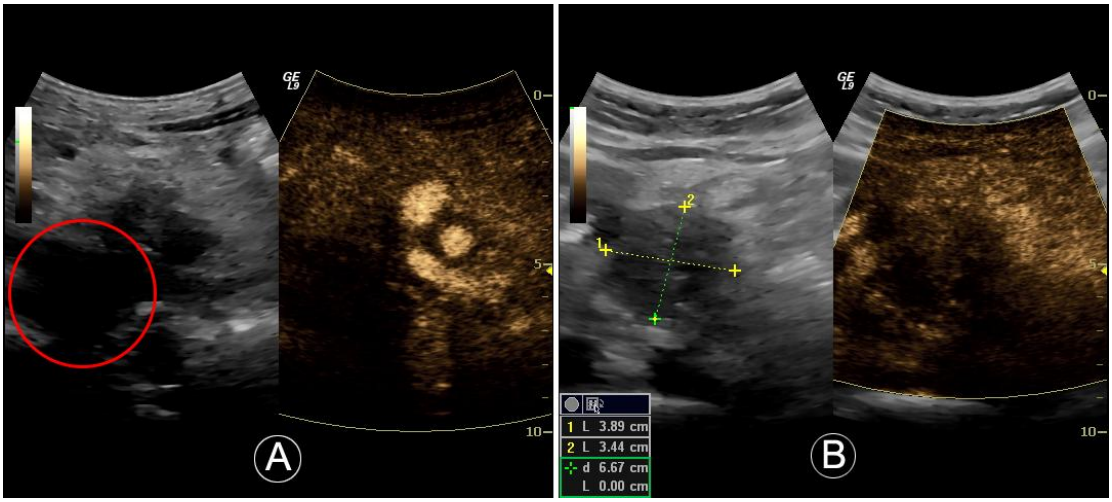

Figure 4: Images captured using customised sonoporation settings using a clinical ultrasound scanner. The dense vasculature in early arterial phase to the right of the main tumour (circled in red) can be seen in panel A. Panel B shows the dimensions of the main tumour, indicated by lines 1 and 2, using the sonoporation settings.

Chemotherapeutic and Microbubble dosage

The recommended chemotherapeutic protocol was followed [50]. This protocol dictates which patients are eligible for chemotherapy and the dosages that can be administered. It includes dosage reduction values depending on platelet and absolute granulocyte count. The chemotherapeutic used, gemcitabine (Gemzar®, Eli Lilly and Company, Indianapolis, IN) was administered once weekly for up to 7 weeks (or until toxicity necessitates reducing or holding a dose), followed by a week of rest from treatment. Subsequent cycles consisted of infusions once weekly for 3 consecutive weeks out of every 4 weeks. Our protocol used the Eastern Cooperative Oncology Group (ECOG) performance status as a measure of the clinical condition [51]. The ECOG performance status ranges from 0–5, where 0 denotes a "*fully active patient able to carry on all pre-disease performance without restriction*", and 5 denotes a "*dead*" patient. Chemotherapy was halted if the patient exceeded a grade of 2 that states the patient is "*ambulatory and capable of all self-care but unable to carry out any works activities. Up and about more than 50% of waking hours.*" The ECOG guidelines can be considered as a measure of how "healthy" a patient is. We used the ECOG guidelines to monitor the effectiveness of the combined treatment *i.e.,* the longer a patient stays below an ECOG grade of 3, the more effective the treatment is considered.

A single treatment cycle is defined as a single infusion of chemotherapeutic followed by ultrasound and microbubble treatment. The week pause was not counted as a treatment cycle. Once the granulocyte or platelet count was permanently too low, or the patient surpassed an ECOG performance status grade of 2, no more treatment was administered.

Gemcitabine was administered by intravenous infusion at a dose of 1000 mg/m^2 over 30 minutes. The start of the chemotherapeutic delivery is defined as $T = 0\,\text{min}$. During the last 10 minutes ($T = 20\,\text{min}$) of chemotherapeutic delivery, diagnostic imaging was performed in standard abdominal imaging mode and the tumour was located. Here the tumour dimensions were measured with ultrasonography. Once the tumour was located, a custom made clamp was used to lock the probe in position and the clinical scanner was switched to therapeutic settings (Fig 5). As the maximum systemic concentration of the chemotherapeutic starts at the finish of delivery ($T = 30\,\text{min}$) this was chosen as the initiation point for the ultrasound treatment. Clinically approved SonoVue® (Bracco Imaging Scandinavia AB, Oslo, Norway) ultrasound contrast agent was used as the microbubble for sonoporation. To ensure microbubbles were present throughout the whole treatment 0.5 mL of contrast agent followed by 5 mL saline were injected every 3.5 min, *i.e.,* at $T = 30.0, 33.5, 37.0, 40.5, 44.0, 47.5, 51.0, 54.5 \text{ and } 58.0\,\text{min}$. A single vial (4.5 mL) was used throughout each treatment. Treatment was stopped at $T = 61.5\,\text{min}$. The total cumulated ultrasound treatment time was only 18.9 s. This time frame can be seen in Fig. 5A.

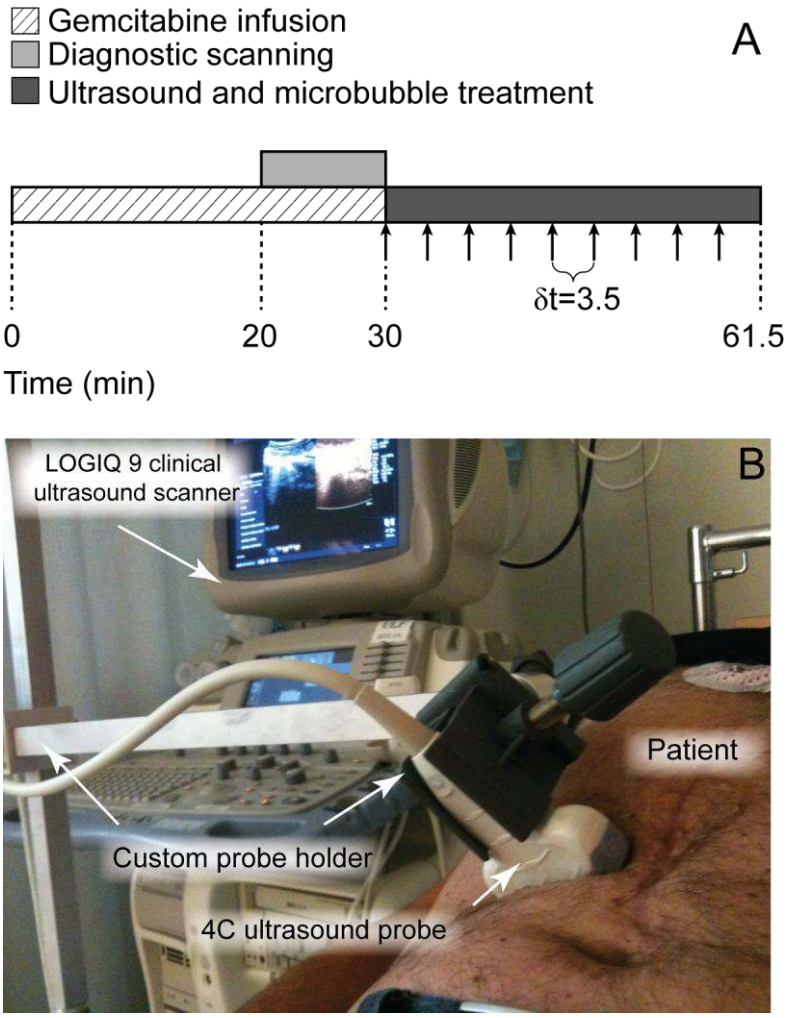

Figure 5: Time frame of each chemotherapy cycle (Panel A) and photograph of probe and custom made probe holder during patient treatment using microbubble sonoporation for pancreatic cancer (Panel B). Panel A shows the time frame for each treatment cycle from the start of the gemcitabine infusion. Arrows indicate intravenous injection time of 0.5 mL SonoVue® followed by a 5-mL intravenous injection of saline. Time between each injection (δt) is 3.5 minutes.

Measurement of disease and tumour progression

The primary measure for evaluating the effectiveness of the treatment was the amount of cycles the patient could undergo. The more treatment cycles the patient underwent, the longer the patient was considered healthy [50, 51]. Furthermore, if the tumour size was reduced substantially in accordance to the Response Evaluation Criteria in Solid Tumours (RECIST) [52], the treatment modality was re-evaluated, *e.g.* transfer to radiation therapy or surgery. This was considered a successful treatment.

Diagnostic ultrasound imaging was performed weekly assessing the tumour size. As Computerised Tomography CT scans are considered the golden standard for following tumour growth [53], every 8 weeks a CT scan was also performed to validate the tumour size. This value was used to follow the tumour progression.

Positron Emission Tomography (PET) imaging was also performed at the start of the treatment to assess the presence of metastasis.

Figure 6 shows the pancreatic adenocarcinoma in patient 5 prior to ultrasound and microbubble treatment as seen by CT and PET imaging modalities.

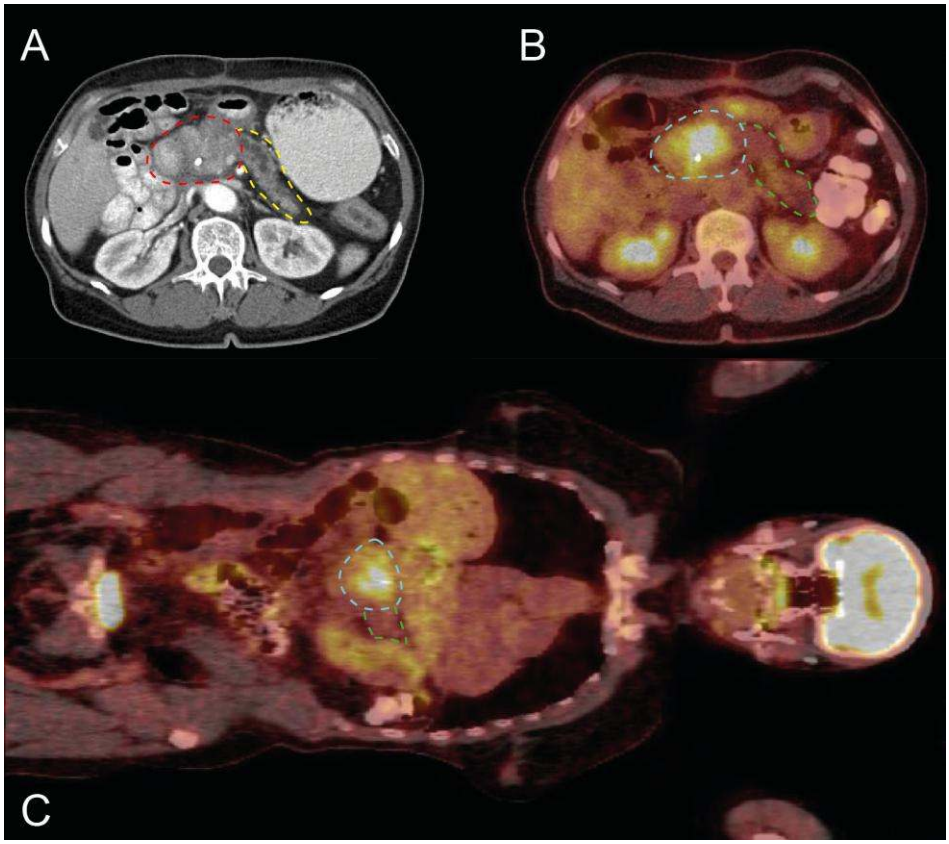

Figure 6. CT (Panel A) and PET (Panels B and C) images of patient 5 showing pancreatic adenocarcinoma prior to treatment. Panel A shows a CT scan in the transverse plane with the primary tumour in the head of the pancreas, and the pancreas indicated by the red and yellow dashed lines respectively. Panels B and C show PET scans in transverse and coronal plane respectively. The location of the tumour can be clearly identified by the brighter colour in the middle of the abdomen. In Panels B and C, the tumour and pancreas are respectively indicated by the blue and green dashed lines. The pancreas tail is behind the large colon in panel C.

274

275 **Treatment group**

276 Patients with inoperable pancreatic cancer and fulfilled the inclusion criteria at the
277 Haukeland University Hospital, Bergen, Norway, who have volunteered to participate,
278 were included. The inclusion critera primarily stated that the patients must be > 18

years of age, a diagnosis of inoperable pancreatic cancer, histologically verified, locally advanced (stage II/III) or metastatic (stage IV) adenocarcinoma of the pancreas, and must be ambulatory with an ECOG performance status between 0 and 2. For this case report a total of five patients were recruited. Table 3 shows the characteristics of the five patients enrolled in this pilot study prior to treatment in addition to the start and end dates of the treatment for every patient.

			Patient 1	Patient 2	Patient 3	Patient 4	Patient 5
Age			66	55	70	68	51
Sex			Male	Male	Female	Female	Female
Pathology Findings			Pancreatic ductal adenocarcinoma				
ECOG Performance			0	1	1	0	1
Biochemistry	ALAT	IU/L	20	55	138	23	66
	LD	IU/L	121	146	153	117	176
	Leuk	$x10^9$ U/L	6.8	3.8	6.9	6.1	11.1
	Neutr	$x10^9$ U/L	4.3	5.8	3.8	3.5	7.1
Tumour Markers	Ca 125		ND	54.1	102	ND	136.6
	Ca 19-9		59	ND	ND	4608	ND
Treatment dates (dd/mm/yyyy)	Start date		06/01/2012	04/04/2012	07/03/2012	22/02/2012	15/02/2012
	End date		26/092012	01/08/2012	11/07/2012	11/05/2012	08/06/2012

Table 3: Patient characteristics prior to treatment. ND denotes non-discernable values. Start and end date of treatment are also stated.

Control group

Taking into account the guidelines for gemcitabine treatment, it can be deduced that the more treatment cycles the patient can undergo, the longer the patient can be considered healthy; hence the more effective the treatment. Once the patient surpasses a Level 2 in the ECOG performance status guidelines, they would no longer receive treatment; this would accordingly define the end of the healthy and ambulatory period. Our control group consisted of 80 patients from 2009-2011 with histology

showing pancreatic adenocarcinoma (matching the same criteria as our patients). These patients received the identical chemotherapy treatment (in accordance to Gemzar guidelines [50]) at Haukeland University Hospital, Bergen, Norway. The control treatments were also discontinued once they surpassed and ECOG performance grade of 2 or their blood counts dropped below the chemotherapy guidelines. Patients who received a different treatment were excluded from the control group. The data was accessed through the internal hospital medical system. The same anonymous data will be available on the Norwegian national cancer registry.

Ethical Considerations

All experiments were performed with approval from the regional ethics committee under reference number 2011/1601/REK vest.

Results and discussion

The beam characterisation showed that the clinical scanner took into account the attenuation of soft tissue when varying the focal depth. This allowed for a good prediction of the ultrasound profile *in-situ* and easy manipulation of the ultrasound intensity and positioning. The "active" area that we assume enhances the chemotherapy effect was long and wide in all cases independent of depth, surpassing the tumour size, allowing a maximum flexibility on treatment area. It has be assumed that there are some fluctuations in the sound field pressures due to tissue property variations, but this should not drastically change the sound field in our case, as acoustic propagation was only though soft tissue. Taking into account the vast range of ultrasound intensities used to induce sonoporation, as seen in literature, we assume

that sonoporation may be occurring at lower or higher acoustic pressures independent of the varying attenuation of tissue. A benefit of using a clinical probe is also that due to the synthetic aperture, objects obscuring the field of view do not affect the beam formation in other areas; hence we can predict the ultrasound dose delivered to our target area.

The image generated using our customised treatment settings allowed easy identification of both microbubbles and tumours. Figure 4A shows clear signs of microbubble presence in the tumour vasculature and surrounding tissue. Figure 4B shows the dimensions of a pancreatic tumour indicating the ease of detecting and aligning the probe to the tumour using the modified settings.

Figure 7 shows the normalised perfusion curve where the arrows indicate the contrast injection time, as measured by the clinical scanner during the first 13 minutes of ultrasound and microbubble treatment. A pseudo-sinusoidal perfusion curve can be seen. Throughout the whole treatment we can see that there are always microbubbles present. By using this pseudo-continuous method we can ensure that there are always microbubbles present without the added complexity of continuous infusion equipment.

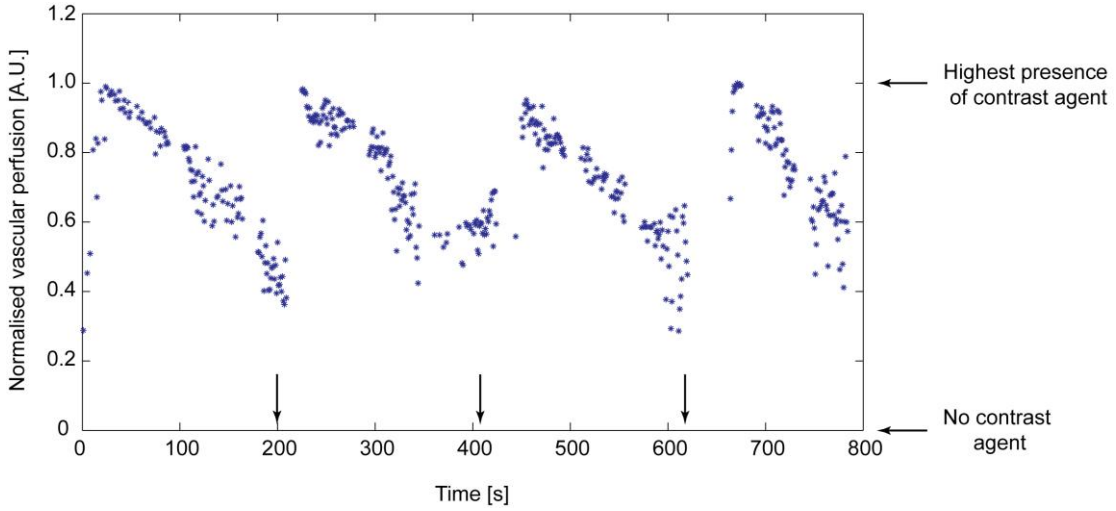

Figure 7: Normalised microbubble presence in tumour locality during the first 800 s of treatment. Arrows indicate contrast injection time.

Our control group, treated with the same chemotherapeutic protocol, received an average of 9±6 treatment cycles. To date all patients participating in this trial have already surpassed this indicating the potential benefit of our combined treatment on a clinical scale with minimal changes to chemotherapy protocols. The patients enrolled in this clinical pilot study received and average of 16±7 treatment cycles.

Figure 8 and Table 3 show the effect of our combined treatment on the tumour size. After 8 weeks two patients showed a tumour diameter reduction. Patient 1 had a temporary tumour reduction from 4.0 cm to 3.1 cm. The next CT image was taken 24 weeks later and showed a growth to 4.6 cm; an increase of 15% from the original tumour size after 32 weeks of treatment. In patient 2, the treatment resulted in a continuous tumour reduction over 16 weeks, a very rare response from chemotherapy alone. As a result of his increased health, after 10 treatment cycles, he was removed from the clinical trial to undergo radiation therapy. As this patient was removed from the trial due to the success of the treatment, a lower number of total and average treatments was seen, reducing the apparent effectiveness of the treatment as a whole.

It should be noted that none of the patients in the control group stopped treatment due to its success but on the contrary, due to their deterioration.

Two patients showed slow tumour growth from the 8th week onwards (patient 3 and patient 4). Patient 5 also had a biopsy verified primary tumour in the pancreas. This was surgically removed but re-occurred with a small tumour in the operation sight and a large metastasis. This indicated that the tumour was at a late stage of development hence a limited response could be expected from the chemotherapeutic. Nevertheless, this patient was also able to receive 11 cycles of treatment.

As pancreatic cancer is such an aggressive form of cancer it is very uncommon to see any decrease in tumour growth from chemotherapy. Our aim was to improve quality of life, to extend the healthy period of life, and conclusively extend the patients survival. If the patient was "healthy" enough (well-defined state in both groups, ECOG performance status 0-2 [51]), they would be able to receive treatment for a longer period. In fact, as long they are ambulatory and capable of all self-care they are able to receive the treatment. Seeing a decrease in the primary tumour size was an added benefit to the increased number of treatment cycles and thereby the anticipated survival.

Patient	Maximum tumour diameter (cm)					Total number of cycles
	Inclusion day	Week 8	Week 16	Week 24	Week 32	
1	4.0	3.1	-	-	4.6	27
2	4.9	3.9	3.6	-	-	10
3	1.5	3.0	3.5	-	-	11
4	2.2	-	2.3	2.9	3.4	16
5	4.0	-	5.5	6.2	-	16

Table 4: Maximum tumour diameter as measured from CT images. Empty values denote skipped CT scans.

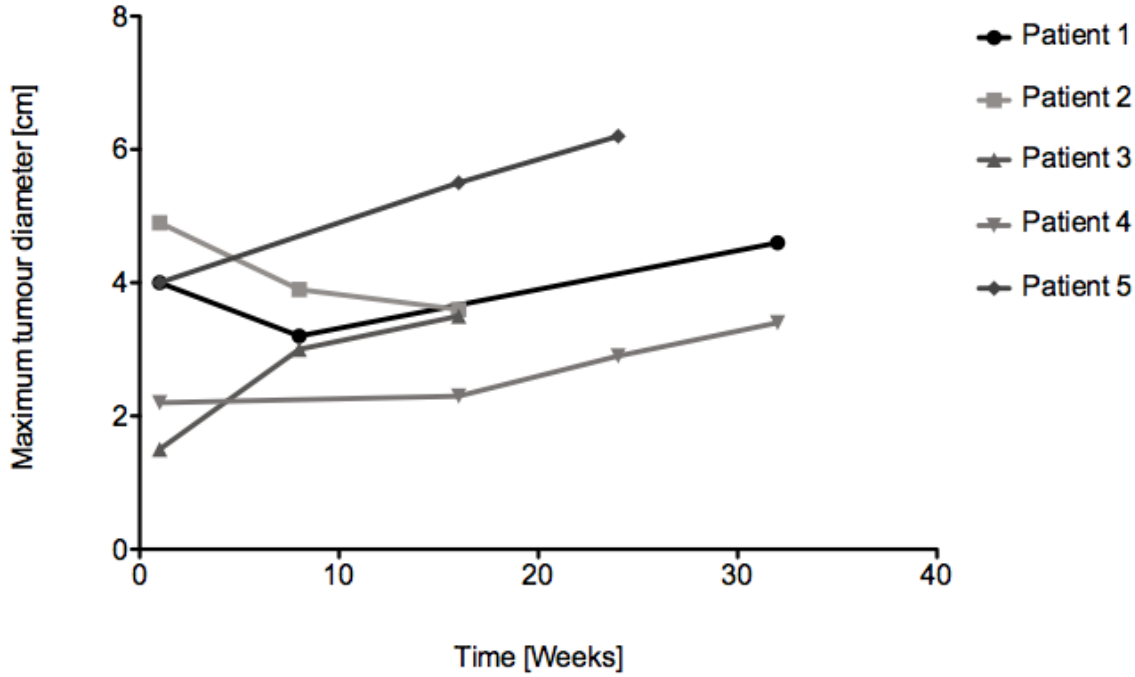

Figure 8: Change in tumour diameter over time measured from CT images in patients with pancreatic malignancy.

The addition of the sonoporation procedure following the standard chemotherapeutic protocol did not add any discomfort to the patients. All patients were very relaxed during the treatment to a state where they could comfortably sleep throughout the whole treatment.

In this study we also aimed to show that it is possible to induce sonoporation in the clinic using existing commercial equipment, whilst fitting in the current safety regulations for the use of diagnostic ultrasound. In our previous work we showed that a duty cycle of 40% was ideal for sonoporation [7, 23]. Here we are using a duty cycle of 1%; hence expecting a small effect of sonoporation. There are many ways to improve this method of therapy such as by increasing the duty cycle from 1% to 40% and introducing targeted microbubbles that could attach to specific cancer cells [40].

The efficacy of our combined treatment should be compared to the efficacy of the current golden standard, the chemotherapeutic gemcitabine alone, where the viability of the patient has been extended by approximately 1 month [3, 4].

Conclusion

Using a clinical diagnostic scanner for therapeutic purposes allows accurate acoustic field alignment ensuring that the desired ultrasound dose reaches the target area. This configuration allows simultaneous visualisation of the microbubbles present whilst treating the pancreatic tumour. In this pilot study, we saw an extended treatment period when comparing to the control group. Furthermore, we did not notice any adverse side effects. Combined ultrasound, microbubble and chemotherapeutic treatment could pave the way for a novel enhanced drug delivery pathways.

412

413 ## Acknowledgements

414 This study has been supported by funds from the Norwegian Cancer Society (NCS)
415 and MedViz (http://medviz.uib.no/), an interdisciplinary research cluster from
416 Haukeland University Hospital, University of Bergen and Christian Michelsen
417 Research AS. We would like to thank Dr. Martin Biermann, Dr. Tormod Bjårnes, Dr.
418 Bjørn Tore Gjertsen, Dr. Anders Molven and Dr. Halfdan Sørbye for their support
419 throughout this project.

420

421

References

[1] World Health Organization. (2012). *World Health Statistics*. Available: http://www.who.int/gho/publications/world_health_statistics/2012/en/index.html

[2] D. Hariharan, A. Saied, and H. M. Kocher, "Analysis of mortality rates for pancreatic cancer across the world," *HPB (Oxford),* vol. **10**, pp. 58-62, (2008).

[3] J. P. Neoptolemos, J. A. Dunn, D. D. Stocken, J. Almond, K. Link, H. Beger, C. Bassi, M. Falconi, P. Pederzoli, C. Dervenis, L. Fernandez-Cruz, F. Lacaine, A. Pap, D. Spooner, D. J. Kerr, H. Friess, M. W. Buchler, and C. European Study Group for Pancreatic, "Adjuvant chemoradiotherapy and chemotherapy in resectable pancreatic cancer: a randomised controlled trial," *Lancet,* vol. **358**, pp. 1576-1585, (2001).

[4] J. P. Neoptolemos, D. D. Stocken, H. Friess, C. Bassi, J. A. Dunn, H. Hickey, H. Beger, L. Fernandez-Cruz, C. Dervenis, F. Lacaine, M. Falconi, P. Pederzoli, A. Pap, D. Spooner, D. J. Kerr, M. W. Buchler, and C. European Study Group for Pancreatic, "A randomized trial of chemoradiotherapy and chemotherapy after resection of pancreatic cancer," *N Engl J Med,* vol. **350**, pp. 1200-1210, (2004).

[5] S. Bao, B. D. Thrall, and D. L. Miller, "Transfection of a reporter plasmid into cultured cells by sonoporation in vitro," *Ultrasound Med. Biol.,* vol. **23**, pp. 953-959, (1997).

[6] A. van Wamel, K. Kooiman, M. Harteveld, M. Emmer, F. J. ten Cate, M. Versluis, and N. de Jong, "Vibrating microbubbles poking individual cells: drug transfer into cells via sonoporation," *J. Control. Release,* vol. **112**, pp. 149-155, (2006).

[7] A. Delalande, S. Kotopoulis, T. Rovers, C. Pichon, and M. Postema, "Sonoporation at a low mechanical index," *Bub. Sci. Eng. Tech.,* vol. **3**, pp. 3-11, (2011).

[8] M. Postema, S. Kotopoulis, A. Delalande, and O. H. Gilja, "Sonoporation: Why microbubbles create pores," *Ultraschall in Med.,* vol. **33**, pp. 97-98, (2012).

[9] N. G. Lee, J. L. Berry, T. C. Lee, A. T. Wang, S. Honowitz, A. L. Murphree, N. Varshney, D. R. Hinton, and A. A. Fawzi, "Sonoporation enhances chemotherapeutic efficacy in retinoblastoma cells in vitro," *Invest Ophthalmol Vis Sci,* vol. **52**, pp. 3868-3873, (2011).

[10] C. X. Deng, F. Sieling, H. Pan, and J. Cui, "Ultrasound-induced cell membrane porosity," *Ultrasound Med Biol,* vol. **30**, pp. 519-526, (2004).

[11] R. K. Schlicher, H. Radhakrishna, T. P. Tolentino, R. P. Apkarian, V. Zarnitsyn, and M. R. Prausnitz, "Mechanism of intracellular delivery by acoustic cavitation," *Ultrasound Med Biol,* vol. **32**, pp. 915-924, (2006).

[12] Y. Z. Zhao, Y. K. Luo, C. T. Lu, J. F. Xu, J. Tang, M. Zhang, Y. Zhang, and H. D. Liang, "Phospholipids-based microbubbles sonoporation pore size and reseal of cell membrane cultured in vitro," *J Drug Target,* vol. **16**, pp. 18-25, (2008).

[13] M. Postema and O. H. Gilja, "Ultrasound-directed drug delivery," *Curr. Pharm. Biotechnol.,* vol. **8**, pp. 355-361, (2007).

[14] M. Postema, O. H. Gilja, and A. van Wamel, "CEUS and sonoporation," in *Fundamentals of Medical Ultrasonics*, M. Postema, Ed., London: Spon press, 2011, pp. 205-217.
[15] M. Postema, S. Kotopoulis, A. Delalande, and O. H. Gilja, "Ultrasound-guided delivery and sonoporation," in *Ultrasound in Gastroenterology. 10-years aniversary of National Center for Ultrasound in Gastroenterology*, 2011, pp. 57-59.
[16] J. M. Escoffre, A. Novell, J. Piron, A. Zeghimi, A. Doinikov, and A. Bouakaz, "Microbubble attenuation and destruction: are they involved in sonoporation efficiency?," *IEEE Trans Ultrason Ferroelectr Freq Control,* vol. **60**, pp. 46-52, (2013).
[17] D. L. Miller and C. Dou, "Membrane damage thresholds for 1- to 10-MHz pulsed ultrasound exposure of phagocytic cells loaded with contrast agent gas bodies in vitro," *Ultrasound Med. Biol.,* vol. **30**, pp. 973-977, (2004).
[18] D. L. Miller and C. Dou, "Membrane damage thresholds for pulsed or continuous ultrasound in phagocytic cells loaded with contrast agent gas bodies," *Ultrasound Med. Biol.,* vol. **30**, pp. 405-411, (2004).
[19] D. L. Miller, C. Dou, and J. Song, "DNA transfer and cell killing in epidermoid cells by diagnostic ultrasound activation of contrast agent gas bodies in vitro," *Ultrasound Med. Biol.,* vol. **29**, pp. 601-607, (2003).
[20] D. L. Miller and J. Quddus, "Sonoporation of monolayer cells by diagnostic ultrasound activation of contrast-agent gas bodies," *Ultrasound Med. Biol.,* vol. **26**, pp. 661-667, (2000).
[21] M. W. Miller, "Gene transfection and drug delivery," *Ultrasound Med. Biol.,* vol. **26**, pp. S59-S62, (2000).
[22] K. Kooiman, M. Harteveld, A. F. W. van der Steen, and N. de Jong, "Sonoporation of endothelial cells by vibrating targeted microbubbles," *J. Control Release,* vol. **154**, pp. 35-41, (2011).
[23] A. Delalande, A. Bouakaz, G. Renault, F. Tabareau, S. Kotopoulis, P. Midoux, B. Arbeille, R. Uzbekov, S. Chakravarti, M. Postema, and C. Pichon, "Ultrasound and microbubble-assisted gene delivery in Achilles tendons: long lasting gene expression and restoration of fibromodulin KO phenotype," *J Control Release,* vol. **156**, pp. 223-230, (2011).
[24] S. M. Nejad, S. H. R. Hosseini, H. Akiyama, and K. Tachibana, "Optical observation of cell sonoporation with low intensity ultrasound," *Biochemical and Biophysical Research Communications,* vol. **413**, pp. 218-223, (2011).
[25] F. Yang, N. Gu, D. Chen, X. Xi, D. Zhang, Y. Li, and J. Wu, "Experimental study on cell self-sealing during sonoporation," *J Control Release,* vol. **131**, pp. 205-210, (2008).
[26] Y. Qiu, C. Zhang, J. Tu, and D. Zhang, "Microbubble-induced sonoporation involved in ultrasound-mediated DNA transfection in vitro at low acoustic pressures," *Journal of Biomechanics,* vol. **45**, pp. 1339-1345, (2012).
[27] M. Matsuo, K. Yamaguchi, L. B. Feril, Jr., H. Endo, K. Ogawa, K. Tachibana, and J. Nakayama, "Synergistic inhibition of malignant melanoma proliferation by melphalan combined with ultrasound and microbubbles," *Ultrason Sonochem,* vol. **18**, pp. 1218-1224, (2011).
[28] N. Lamanauskas, A. Novell, J. M. Escoffre, M. Venslauskas, S. Satkauskas, and A. Bouakaz, "Bleomycin delivery into cancer cells in vitro with ultrasound and SonoVue® or BR14® microbubbles.," *J Drug Target,* vol. **1**, p. [Epub ahead of print], (2013).

[29] Y. Watanabe, A. Aoi, S. Horie, N. Tomita, S. Mori, H. Morikawa, Y. Matsumura, G. Vassaux, and T. Kodama, "Low-intensity ultrasound and microbubbles enhance the antitumor effect of cisplatin," *Cancer Sci,* vol. **99**, pp. 2525-2531, (2008).
[30] J. Wu, J. Pepe, and M. Rincon, "Sonoporation, anti-cancer drug and antibody delivery using ultrasound," *Ultrasonics,* vol. **44**, pp. E21-E25, (2006).
[31] C. Y. Lai, C. H. Wu, C. C.C., and P. C. Li, "Quantitative relations of acoustic inertial cavitation with sonoporation and cell viability," *Ultrasound Med. Biol.,* vol. **32**, pp. 1931-1941, (2006).
[32] D. M. Hallow, A. D. Mahajan, T. E. McCutchen, and M. R. Prausnitz, "Measurement and correlation of acoustic cavitation with cellular bioeffects," *Ultrasound Med. Biol.,* vol. **32**, pp. 1111-1122, (2006).
[33] M. M. Forbes, R. L. Steinberg, and W. D. O'Brien, "Examination of Inertial Cavitation of Optison in Producing Sonoporation of Chinese Hamster Ovary Cells," *Ultrasound in Medicine and Biology,* vol. **34**, pp. 2009-2018, (2008).
[34] J. L. Tlaxca, C. R. Anderson, A. L. Klibanov, B. Lowrey, J. A. Hossack, J. S. Alexander, M. B. Lawrence, and J. J. Rychak, "Analysis of in vitro Transfection by Sonoporation Using Cationic and Neutral Microbubbles," *Ultrasound Med Biol,* vol. **36**, pp. 1907-1918, (2010).
[35] C. D. Ohl and B. Wolfrum, "Detachment and sonoporation of adherent HeLa-cells by shock wave-induced cavitation," *Biochimica Et Biophysica Acta-General Subjects,* vol. **1624**, pp. 131-138, (2003).
[36] D. L. Miller and C. Y. Dou, "Induction of Apoptosis in Sonoporation and Ultrasonic Gene Transfer," *Ultrasound in Medicine and Biology,* vol. **35**, pp. 144-154, (2009).
[37] M. Postema and O. H. Gilja, "Jetting does not cause sonoporation," *Biomed. Eng.,* vol. **55**, pp. S19-S20, (2010).
[38] B. Geers, H. Dewitte, S. C. De Smedt, and I. Lentacker, "Crucial factors and emerging concepts in ultrasound-triggered drug delivery," *J Control Release,* vol. **164**, pp. 248-255, (2012).
[39] F. G. Erchinger, G. Dimcevski, T. Engjom, and O. H. Gilja, "Transabdominal ultrasonography of the pancreas: basic and new aspects," *Imaging Med.,* vol. **3**, pp. 412-422, (2011).
[40] M. Postema and O. H. Gilja, "Contrast-enchanced and targeted ultrasound," *World J. Gastroenterol.,* vol. **17**, pp. 28-41, (2011).
[41] F. Piscaglia, C. Nolsoe, C. F. Dietrich, D. O. Cosgrove, O. H. Gilja, M. Bachmann Nielsen, T. Albrecht, L. Barozzi, M. Bertolotto, O. Catalano, M. Claudon, D. A. Clevert, J. M. Correas, M. D'Onofrio, F. M. Drudi, J. Eyding, M. Giovannini, M. Hocke, A. Ignee, E. M. Jung, A. S. Klauser, N. Lassau, E. Leen, G. Mathis, A. Saftoiu, G. Seidel, P. S. Sidhu, G. ter Haar, D. Timmerman, and H. P. Weskott, "The EFSUMB Guidelines and Recommendations on the Clinical Practice of Contrast Enhanced Ultrasound (CEUS): update 2011 on non-hepatic applications," *Ultraschall in Med.,* vol. **33**, pp. 33-59, (2012).
[42] M. Postema, *Fundamentals of medical ultrasonics*. Milton Park, Abingdon, Oxon ; New York: Spon Press, 2011.
[43] B. Gerold, S. Kotopoulis, M. C., D. McGloin, M. Postema, and P. Prentice, "Laser-nucleated acoustic cavitation in focused ultrasound," *Rev. Sci. Instrum.,* vol. **82**, p. 044908, (2011).

[44] U.S. Department of Health and Human Services. Food and Drug Administration, "Information for Manufacturers Seeking Marketing Clearance of Diagnostic Ultrasound Systems and Transducers," 2008.
[45] International Electrotechnical Commision, "Ultrasonics - Hydrophones - Part 2: Calibration for ultrasonic fields up to 40 MHz," 2013.
[46] J. A. Jensen, S. I. Nikolov, K. L. Gammelmark, and M. H. Pedersen, "Synthetic aperture ultrasound imaging," *Ultrasonics,* vol. **44 Suppl 1**, pp. e5-15, (2006).
[47] E. Quaia, "Microbubble ultrasound contrast agents: an update," *European Radiology,* vol. **17**, pp. 1995-2008, (2007).
[48] British Medical Ultrasound Society, *Guidelines for the safe use of diagnostic ultrasound equipment*, 2000.
[49] S. B. Barnett, G. R. Ter Haar, M. C. Ziskin, H. D. Rott, F. A. Duck, and K. Maeda, "International recommendations and guidelines for the safe use of diagnostic ultrasound in medicine," *Ultrasound Med Biol,* vol. **26**, pp. 355-366, (2000).
[50] Eli Lilly and Company. (2010). *Highlights of prescribing information - Gemzar*. Available: http://pi.lilly.com/us/gemzar.pdf
[51] M. M. Oken, R. H. Creech, D. C. Tormey, J. Horton, T. E. Davis, E. T. Mcfadden, and P. P. Carbone, "Toxicity and Response Criteria of the Eastern-Cooperative-Oncology-Group," *American Journal of Clinical Oncology-Cancer Clinical Trials,* vol. **5**, pp. 649-655, (1982).
[52] E. A. Eisenhauer, P. Therasse, J. Bogaerts, L. H. Schwartz, D. Sargent, R. Ford, J. Dancey, S. Arbuck, S. Gwyther, M. Mooney, L. Rubinstein, L. Shankar, L. Dodd, R. Kaplan, D. Lacombe, and J. Verweij, "New response evaluation criteria in solid tumours: Revised RECIST guideline (version 1.1)," *European Journal of Cancer,* vol. **45**, pp. 228-247, (2009).
[53] S. A. Sohaib, B. Turner, J. A. Hanson, M. Farquharson, R. T. Oliver, and R. H. Reznek, "CT assessment of tumour response to treatment: comparison of linear, cross-sectional and volumetric measures of tumour size," *Br J Radiol,* vol. **73**, pp. 1178-1184, (2000).